Appl Petrochem Res (2015) 5:181–197
DOI 10.1007/s13203-015-0097-y

ORIGINAL ARTICLE

Citric acid-assisted synthesis of γ-alumina-supported high loading CoMo sulfide catalysts for the hydrodesulfurization (HDS) and hydrodenitrogenation (HDN) reactions

Sergio L. González-Cortés · Yangdong Qian · Hamid A. Almegren · Tiancun Xiao · Vladimir L. Kuznetsov · Peter P. Edwards

Received: 31 December 2014 / Accepted: 25 January 2015 / Published online: 10 February 2015

Abstract In the present work, the effect of the citric acid (i.e., adsorption-assisting agent) and the thermal treatment over the citric acid-synthesized CoMo catalyst precursors were investigated. The catalysts were prepared by wet co-impregnation of γ-alumina extrude with citric acid-containing CoMo aqueous solution in acid medium (pH = 2–3) and treated at various temperatures (typically between 110 and 400 °C) in an air atmosphere. The γ-alumina-supported CoMo sulfide catalysts were evaluated using two different feeds (a model feedstock containing various S and N compounds (hereafter feed 1) and a real feedstock (hereafter feed 2). It was found that the synthesis of alumina-supported high loading CoMo catalyst precursor by wet co-impregnation using citric acid as chelating agent in the CoMo impregnation solution takes place mainly through the uniform deposition–precipitation of Co aqueous complex and Mo citrate onto alumina. This process leads to the formation of nanodispersed Co and Mo species that effectively mitigate the formation of β-$CoMoO_4$ during the thermal treatment at high temperature (i.e., 350 °C). The decomposition reaction of Co aqueous-complex and Mo citrate deposited on alumina started at 220 °C. The gradual degradation of the whole metal citrate with increasing treatment temperature decreased the catalyst activity because of the apparent formation of poorly reducible mixed-metal oxides in the catalyst precursor. The use of citric acid to synthesize the CoMo formulations enhances not only the C–S bond scission through the direct desulfurization pathway, but also the hydrogenation route.

Keywords CoMo sulfide catalyst · Citric acid · Wet impregnation · HDS catalyst · HDN catalysts

S. L. González-Cortés (✉) · Y. Qian · T. Xiao (✉) · V. L. Kuznetsov · P. P. Edwards (✉)
Inorganic Chemistry Laboratory, Department of Chemistry, KACST-Oxford Petrochemical Research Centre (KOPRC), University of Oxford, Oxford OX1 3QR, UK
e-mail: sergio.gonzalez-cortes@chem.ox.ac.uk

T. Xiao
e-mail: xiao.tiancun@chem.ox.ac.uk

P. P. Edwards
e-mail: peter.edwards@chem.ox.ac.uk

H. A. Almegren
Petrochemicals Research Institute (PRI), King Abdulaziz City of Science and Technology (KACST), P.O. Box 6086, Riyadh 11442, Saudi Arabia

Introduction

It is well-established that the combustion of fossil fuels emits harmful gases and compounds into the atmosphere that produce long-term disease in the living organisms and also the greenhouse effect. Major emissions of NO_x, SO_x, CO_2 and particulate matter are the causes of most concern for pollution in our environment. To alleviate their impact, stringent environmental regulations have been introduced in many developed countries to reduce the sulfur and aromatic contents in the transportation fuels with the aim of lowering harmful exhaust emissions and enhancing air quality. The relatively low sulfur concentrations that need to be achieved in transportation fuels necessitate the ultra-deep treatment of the fuel feed stream. This is a highly demanding and energy-intensive process because the global market for diesel fuel is steadily increasing whilst the quality of the feed streams available is markedly declining; low-grade feeds or even alternative raw materials may need to be processed to meet the ever-increasing additional demand of ultraclean fuel required for

transportation [36, 42]. Thereby, the development of advanced hydrotreatment catalysts is of paramount importance not only in the reduction of some environmental pollution (i.e., aromatics, S and N compounds) but also in the upgrading process of low-grade feedstock.

The synthesis of supported catalysts by wet or incipient wetness impregnation of porous support bodies with a solution of the metal precursor followed by evaporation of the solvent and subsequent decomposition of the metal precursor by calcination is one of the most important and common process to produce heterogeneous catalysts in industrial practice [1, 4]. Nevertheless, the fundamental phenomena involved upon impregnation, drying and even calcination are rather complex and difficult to be rationalised in a simple model. A limited interaction between the metal precursor and the support body can conduct to the redistribution of the active phase during the drying and calcination steps, causing the migration of the active phase toward the external edge of the support body to produce egg-shell catalyst [13, 31, 45]. Therefore, the optimization of the interaction between the metal precursor and the support is crucial to tune the distribution of the active component within the support body and hence the catalyst performance. Nowadays, a fairly common strategy to control the metal precursor–support interaction during the synthesis of hydrodesulfurization (HDS) catalysts is adding in the impregnation solution chelating agents or organic additives, which have showed a marked enhancement in the catalytic removal of S-containing compounds [17, 21, 22, 33, 35, 38, 40]. It is fairly well-established that two different Co–Mo–S type phase can be produced on alumina surface: (1) A type I Co–Mo–S phase not fully sulphided, which contains some Mo–O–Al linkages with the support and (2) a type II Co–Mo–S phase fully sulphided, which shows weak interaction (Van der Waals) with the support and higher activity than that of type I [20, 43]. The use of an organic compound upon impregnation process can facilitate the formation of type II Co–Mo–S phase by decreasing metal sulphide-support interaction, which could also facilitate hydrogen transfer reactions.

Citric acid (CA) as chelating agent was used to synthesize the SBA-15-supported NiMo sulfide catalysts [25], which were evaluated in the HDS reaction of dibenzothiophene (DBT) and 4,6-dimethyldibezothiophene (4,6-DMDBT). The catalyst precursors were prepared by co-impregnation of SBA-15 with Ni, Mo and CA solution at two different pH values (i.e., 1 and 9 units) and pre-sulfided ex situ at 400 °C. It was found that the SBA-15-supported NiMo formulations were more active for the HDS reaction of DBT than the equivalent catalysts synthesized in basic aqueous solutions. Furthermore, the dried and calcined catalysts synthesized in acid medium were selective toward the hydrogenation pathway of HDS reactions. The selectivity of the catalysts prepared from basic solutions (pH = 9) was strongly affected by the thermal treatment [25]. An unexpected promotion of the direct desulfurization route of DBT reaction with increasing citric acid concentration was also observed [44]. Citric acid as chelating agent has been also employed in the synthesis of HY zeolite–alumina-supported CoMoP sulfide catalysts [11, 12]. This catalyst was synthesized by simultaneous impregnation of aqueous solution containing Co, Mo, orthophosphoric acid and citric acid over HY zeolite-modified alumina and air-drying without calcination. It was found that the presence of citric acid prevents the sulfidation of cobalt and promotes the synthesis of molybdenum sulfide at low temperature, hence facilitating the formation of the type-II Co–Mo–S structure. Furthermore, the HY zeolite–alumina-supported CoMoP sulfide catalyst showed under commercial operation conditions excellent activity and stability. The synthesis, characterization and catalytic performance of alumina-supported Co–Mo citrate in the ultra-deep HDS reaction of straight-rung gas oil was also recently examined [24, 37]. The oxidic catalyst precursor consists of tretrameric Mo^{6+} citrate anions with Co^{2+} cation coordinated to the carboxyl groups and terminal oxygen atoms deposited on alumina, whose maximum HDS activity was obtained in the catalyst thermally treated at 220 °C.

It is well-established in the literature that the use of citric acid as chelating agent can give additional benefit to the HDS catalyst performance as long as the sulfidation is carried out over the catalyst precursors previously treated at low temperatures to preserve the chelating effect over Co (or Ni) and Mo species. However, there is limited understanding about the potential degradation of the Co-Mo citrate complex upon the impregnation process over alumina surface and its decomposition during the thermal treatment of the catalyst precursor and its possible influence over the catalyst stability. In the present study, we tried to gain further insight into the deposition of high loading of Co and Mo citrate species on alumina surface and their evolution during the thermal treatment by characterizing and testing a series of CoMo catalysts. They were synthesized by wet co-impregnation of alumina body with citric acid-containing CoMo aqueous solution. Two different feeds (a model one containing various S and N compounds—feed 1 and a real feedstock—feed 2) are employed to find out the influence of the chelating agent not only on the HDS reactions but also in the HDN reactions. It is envisaged that the deposition of high loading of CoMo on alumina by citric acid-assisted synthesis and the formation of amorphous and nano-dispersed Co and Mo species that effectively mitigate the production of mixed-metal oxides during the calcination can generate new opportunities to develop advanced hydrotreating catalysts for the upgrading of low-grade feedstock.

Experimental

Catalyst preparation

The γ-alumina-supported 6 wt. % CoO, 24 wt. % MoO_3 catalyst precursors were prepared by wet co-impregnation. Initially, an impregnation solution containing ammonium heptamolybdate tetrahydrate (Sigma-Aldrich), cobalt (II) carbonate hydrate (Sigma-Aldrich) and citric acid monohydrate (Sigma-Aldrich, 99 %) in deionised water was prepared. This solution contains [Co] = 0.4 mol L^{-1}, [Mo] = 0.8 mol L^{-1}, [CA] = 0.8 mol L^{-1} and a resultant pH between 2.4 and 2.6. The extruded γ-Al_2O_3 support (17.5 g) (1.5 mm of diameter, 5–10 mm of length and 240 m^2 g^{-1}) previously dried at 110 °C was then added to 100-mL beaker containing the impregnation solution. The solid was fully wetted for a period of 4–24 h. Excess impregnation solution was used, typically between 50 and 100 % relative to the pickup volume of the support (ca. 1 mL g^{-1}). The impregnated catalyst was separated from the excess of impregnation by filtration. Subsequently, the sample was dried at 110 °C for 6 h and re-impregnated under similar conditions to achieve the required loading of MoO_3 (ca. 24 wt. %) and CoO (6 wt. %). Finally, the sample was thermally treated at the required temperature condition (RT/Temp/hold: 1 °C min^{-1} @ 110–350 °C @ 6 h). The nominal CoMo composition was determined by the pickup volume and the experimental composition was determined by inductively coupled plasma atomic emission spectroscopy (ICP–AES).

Catalyst characterization

Simultaneous differential scanning calorimetry (DSC) and thermogravimetric analysis (TGA) were carried out on a SDT (Simultaneous DSC-TGA) Q600 instrument. TGA-DSC profiles were recorded from room temperature to 750 °C, using a 20 cm^3 min^{-1} dry air flow and 5 °C min^{-1} heating rate. For each analysis between 25 and 35 mg of sample was loaded into a small alumina crucible, using alumina as reference.

The textural properties (i.e., surface area, pore volume and pore distribution) of the catalyst oxide precursor were carried out by nitrogen physi-sorption at the nitrogen-liquid temperature (−196 °C). The sample (i.e., 0.150–0.200 g) was initially degassed at room temperature under vacuum (ca. 1×10^{-3} bar) for 2 h. Then the adsorbed volume of nitrogen at different relative pressure (P/Po) was measured to obtain an isotherm curve. It was obtained specific surface area with the Brunauer, Emmett, Teller (BET) method whereas pore volume and pore distribution were found out with the Barret–Joyner–Halenda (BJH) method [46].

The Raman spectra of the oxide precursors were recorded in a Jobin–Yvon Labram spectrometer with a 632 nm HeNe laser, run in a back-scattered co-focal arrangement. The solid samples were pressed in a microscope slide; with a 30 s scanning time and 2 cm^{-1} resolution. Each catalyst surface was probed at several points to explore homogeneity of the sample and reproducibility of the data.

Temperature-programmed reduction (TPR) and also temperature-programmed oxidation (TPO) coupled to mass spectrometer (MS) to analyse the gas evolution from the alumina-supported CA–Co–Mo oxide precursors was carried out on a Micrometrics AutoChem II 2,920 instrument. About 120–150 mg of the solid samples was pre-treated before analysis with a 50 cm^3 min^{-1} He flow rate, from room temperature up to 120 °C for 30 min. The sample was then cooled to room temperature and the TPR profiles were obtained using 10 % H_2 in Ar (50 cm^3 min^{-1}) whilst dried air flowing was used for TPO analysis at 10 °C min^{-1} heating rate from room temperature up to 950 °C.

The crystalline phases of the oxide catalyst precursors were identified by powder X-ray diffraction (XRD) in a Philips PW1710 diffractometer equipped with an X-ray tube (Cu Kα radiation $\lambda = 1.5406$ Å; 40 kV, 30 mA). The samples were prepared by grinding a small amount of each specimen using an agate mortar and pestle and then loaded into a flat sample holder. The data were collected in θ/θ reflection mode, from 20^o to 80^o of 2θ.

High resolution transmission electron microscopy (HRTEM) was carried out using a JEOL 4000FX electron microscope with a 400 kV accelerating voltage. Bimetallic sulfurized catalysts were ground into a fine powder and dispersed in AR-grade chloroform. Then, they were placed in an ultrasonic bath for ca. 15 min, before a drop of the suspension was put on a lacey carbon-coated copper grid (Agar, 20 mesh). At least four representative images were taken for the sample.

Catalytic evaluation of the CoMo citrate-prepared catalysts and commercial CoMo sulfide catalysts

The catalyst (particle size between 250 and 500 μm) mixed with equal volume and comparable particle size of silicon carbide (SiC) was loaded into a tube reactor. The solid sample was initially treated with N_2 flow (50 cm^3 min^{-1}) at 120 °C for 2 h to remove moisture. Then, the hydrotreating unit was pressurized to 3.0 MPa of hydrogen and the catalyst soaked with sulfiding agent (i.e., middle distillate spiked with dimethyl disulfide to total sulfur content of 4 wt. %) and hydrogen flow for 60 min. The liquid (sulfiding agent or feedstock) was continuously fed into the reactor using a Series II high pressure pump

operating in the mode of volumetric flow. Hydrogen and feedstock were brought in contact in the co-current mode. The liquid-phase presulfiding or sulfidation was carried out at a liquid hour space velocity (LHSV) of 7.2 h^{-1} (or 1.2 h^{-1}); H_2/oil volume ratio of 250 N m^3 m^{-3}; 3.5 MPa of hydrogen and 340–350 °C. The temperature was increased at 0.5 °C min^{-1}–240 °C and kept it for 60 min. The temperature was then further increased at 0.5 °C min^{-1}–350 °C and kept at 350 °C for 8 h. After that period, the catalyst bed temperature decreased to 220 °C under sulfiding agent and H_2 flow condition. Then, the hydrogen pressure, the flows of hydrogen and feedstock were set according to the required reaction condition whereas the catalyst bed was increased to reaction temperature at a 0.5 °C min^{-1} heating rate.

The sulfur and nitrogen contents in the liquid products were determined using an Antek 9000VNS instrument whereas the boiling point range and aromatic contents were determined by simulated distillation and gas chromatography, respectively. The calculation of the cetane index was based on the fuel gravity and mid-boiling range for the fuel and liquid products, according to the ASTM (American Society for Testing and Materials) method D-4737A. The catalytic tests showed liquid yield ca. 99 % of liquid recovery. Approximately, 1 wt. % of the product was lost as consequence of the gas product formation (i.e., C_1, C_2, C_3, C_4) as was confirmed by gas chromatography.

The catalytic performances of Al_2O_3-supported CoMo sulphide catalysts were evaluated on two different feedstocks, whose properties are listed in Table 1. The concentrations of nitrogen and aromatics markedly differ whilst sulphur is comparable in these two feeds. It is worth remarking that the feed 1 (i.e., model feed) comprises dibenzothiophene (3,500 wppm), 4,6-dimethyldibenzothiophene (750 wppm), quinoline (1,000 wppm)and fluorene 20,000 wppm) in decalin as solvent. The feed 2 corresponds to a blend of straight run gas oil and gas oil.

Table 1 Compositions and physical properties for various feedstocks

Feedstock properties	Feed 1	Feed 2
Sulfur/ug.g[1]	4,250	5,900
Nitrogen/ug g*	1,000	80
Density (15°C)/g cm^{-3}	0.89	0.84
Boiling point range/°C	187[a]	139–446
Mono-aromatics/wt. %	0	15.7
Di-aromatics/wt. %	0	10
Poly-aromatics/wt. %	2	1.5
Total aromatics/wt. %	2	27.2
Other HCs/wt. %	98	72.8
Cetane index	~	45.2

[a] Based on the boiling point of the solvent

Result and discussion

Characterization of alumina-supported Co, Mo, CoMo and citric acid by various techniques

To evaluate the potential effect of citric acid (CA) over the thermal decomposition of CoMo catalyst a series of citric acid-containing alumina-supported Co, Mo and CoMo samples were synthesized and then characterized by thermogravimetric analysis (TGA) and differential scanning calorimetry (DSC) (Fig. 1).

It is worth indicating that the nominal CA content in the monometallic samples (i.e., Co and Mo) was half of the overall amount used in the synthesis of the bimetallic formulation (i.e., CoMo) and that deposited on alumina (i.e., 32.5 wt. % CA/Al_2O_3). In Table 2 is summarized the weight losses of the citric acid-synthesized samples in dry air flow upon increasing the temperature.

The TG (1a) and DTG (1b) profiles show a first broad stage with a maximum temperature between 80 and 100 °C and a weight loss (WL) between 3.0 and 7.6 wt. % (Table 2). This stage is assigned to the desorption of water molecules from the alumina surface [9, 17, 39] and the partial dehydration of citric acid on alumina, particularly for the CA/Al_2O_3 and Mo + CA/Al_2O_3 samples. Note, however, that the Co-containing catalysts displayed a slightly higher maximum temperature (i.e., 99 and 92 °C) and significantly higher WL (i.e., 7.6 and 7.5 wt. %), which is tentatively attributed to water of crystallization present in the crystalline framework of cobalt citrate complex. The major second WL for CA/Al_2O_3, Mo + CA/Al_2O_3 and CoMo + CA/Al_2O_3 samples reached a maximum temperature at 185, 215 and 225 °C, respectively. This stage is tentatively attributed to a complex series of overlapping chemical reactions involving not only the partial dehydroxylation-decomposition of citric acid and metal-citrate complex [41, 47], but also the partial dehydroxylation of alumina [26]. A third broad weight loss at temperatures above 300 °C is likely associated with the evolution of remaining residue of citric acid and also dehydroxylation of alumina. The Co + CA/Al_2O_3 sample, on the other hand, showed a TG profile markedly different than Mo-containing samples. Indeed, the second WL was only 5.9 wt. % at 250 °C, whilst the major WL (i.e., 14.3 wt. %) occurred at higher temperature (i.e., 290 °C) that those required for the other samples (i.e., 185–225 °C) (see Table 2). It should be mentioned that the total weight loss (TWL) coincided with the expected (theoretical) weight loss for CA/Al_2O_3 and Mo + CA/Al_2O_3 samples, assuming the full decomposition of citric acid and the formation of molybdenum trioxide. On the other hand, the TWL for the Co-containing samples are consistent with the expected WL as long as the weight losses at temperatures below

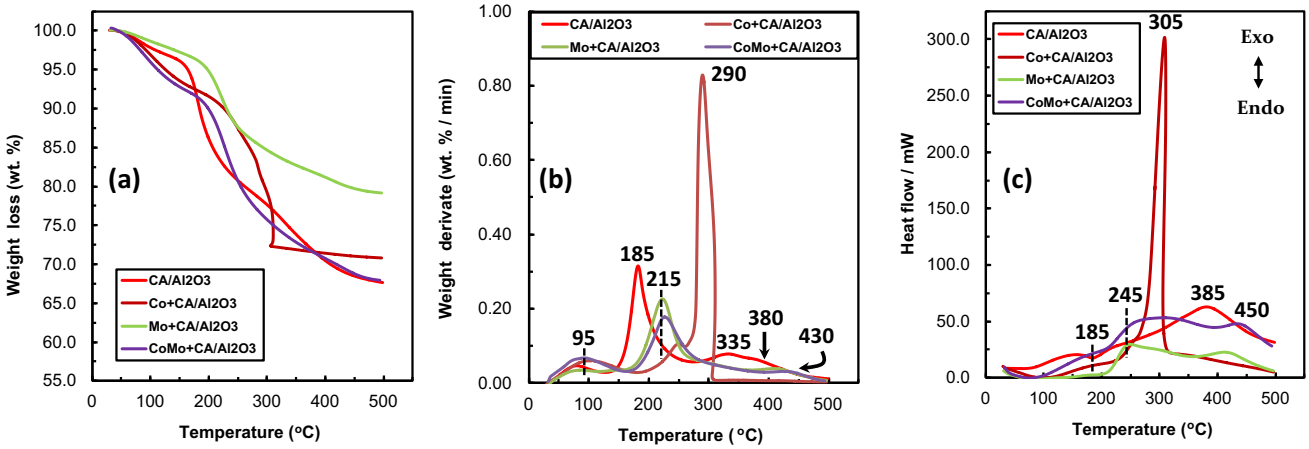

Fig. 1 Thermogravimetric analysis (**a**), differential thermogravimetric analysis (**b**) and differential scanning calorimetry (**c**) for the citric acid-containing alumina-supported Co, Mo and CoMo catalysts

Table 2 Maximum temperatures, main weight losses and overall weight losses for the citric acid-containing alumina-supported Co, Mo and CoMo catalysts treated at 110 °C

Catalyst	Ti (°C)	WLj (wt. %)	T_2 (°C)	WL_2 (wt. %)	T_3 (°C)	WL_3 (wt. %)	TWL (wt. %)
$CA/A1_20_3$	80	3.0	185	16.9	335	12.4	32.3
Co + CA/AIA	99	7.6	250	5.9	290	14.3	27.8
Mo + CA/Al_20_3	85	2.0	215	14.6	430	3.6	20.2
CoMo + CA/Al_20_3	92	7.5	225	19.6	430	4.8	32.0

100 °C were excluded (Table 2), indicating that these samples presented a high degree of crystallization water most likely due to the formation of hydrate cobalt citrate.

The DSC curves for the citric acid-containing samples (Fig. 1c), on the other hand, exhibit a weak endothermic peak at about 85–100 °C associated to the dehydration reactions in agreement with the weight losses determined by TGA. The alumina-deposited CA sample also showed a fairly well-defined endothermic stage at 185 °C. According to Wyrzykowski and co-workers, this peak can be attributed to the melting/decomposition temperature of *trans*-aconitic acid produced from the dehydration reaction of citric acid [47]. Note that this peak is not seen in the other analysed samples because of unavailability of citric acid molecules. No endothermic peak at 153–156 °C associated with the melting point of citric acid was detected. However, a broad exothermic peak centred at 385 °C attributed to the oxidation of remaining residue of citric acid was produced. On the other hand, the γ-alumina-supported Co citrate formulation exhibited a very strong exothermic peak, whose maximum temperature (i.e., 305 °C) coincides fairly well with its maximum weight loss as consequence of the violent combustion reaction into a relatively narrow range of temperature. A similar exothermic stage upon the combustion synthesis of Co_3O_4/γ-Al_2O_3 catalysts for the total oxidation of methane using citric acid as fuel was observed elsewhere [48]. Note that the DSC profile for the CoMo + CA/Al_2O_3 sample showed two broad and weak exothermic peaks whose maximum temperatures are shifted toward higher values (i.e., ca. 10–20 °C) relative to Mo + CA/Al_2O_3 DSC profile, likely due to a Co-Citrate-Mo interaction. Indeed, the presence of Mo attenuates the violent exothermic combustion reaction of the Co + CA/γ-alumina sample. This finding could be indicative of either the possible formation of Co-Mo citrate complex [24, 37] or a selective Mo-citrate interaction relative to Co-citrate interaction. The aforementioned TGA and DSC findings clearly evidence that the citric acid strongly affects the thermal decomposition of alumina-supported CoMo catalyst. According to previous reports [2, 3], citric acid can react with (poly) molybdate and hexaaquo cobalt (II) complex in aqueous solution and hence the formation of metal citrate in the monometallic samples could be expected, assuming no complex degradation upon impregnation process. The violent exothermic reaction combined with a major WL for Co + CA/Al_2O_3 at higher temperature than that for Mo + CA/Al_2O_3 confirms the effective Co-citrate interaction through the chelating effect. On the other hand, the bimetallic formulation (i.e., CoMo + CA/Al_2O_3) showed fairly comparable thermal decomposition profiles (i.e., TGA and DSC) that Mo + CA/Al_2O_3 sample despite the presence of Co cation.

Apparently, the presence of (poly)molybdate species in the bimetallic formulation strongly hindered the cobalt–citrate interaction.

To assess the calcination temperature effect over thermal decomposition of citric acid-containing alumina-supported CoMo catalysts, three samples treated at 110, 220 and 350 °C were analysed by TPO–MS (Fig. 2). Note that there is no water evolution at temperatures below 150 °C because of the in situ sample pre-treatment at 120 °C before the TPO–MS analysis (Fig. 2a). However, the alumina-supported CoMo citrate catalyst dried at 110 °C showed a major and wide peak at 230 °C, whose intensity and overall area decreased, approximately 58 % after the thermal treatment at 220 °C. A reduction of nearly 35 % of the overall curve area was obtained in the sample calcined at 350 °C. Note also that the maximum water evolution is shifted to higher temperatures as increasing the treatment temperature of the alumina-supported CoMo citrate catalysts. The CoMo catalyst treated at 350 °C showed a small peak at 205 °C due to water produced from the dehydroxylation of alumina [26]. The TPO-MS profiles for the CO_2 evolution also showed an important diminution of the overall curve area and shift of the maximum CO_2 response toward higher temperatures as increasing the treatment temperature (Fig. 2b). The evolved H_2O and CO_2 took place into a similar range of temperatures (i.e., 150–600 °C), suggesting that both citric acid dehydration and decarboxylation reactions occur simultaneously. We should also remark that the evolved CO_2 after treating the sample at 350 °C is related to the oxidation of residual carbonaceous material as the evolved H_2O is most likely associated to the dehydroxylation reaction of alumina [26]. Considering the findings from the TPO–MS and the TGA–DSC analysis, one can infer that the major WL centred at 215–225 °C for Mo + CA/Al_2O_3 and CoMo + CA/Al_2O_3 are mainly associated with the dehydroxylation/dehydration and decarboxylation reactions whilst the WL at ca. 430 °C is mainly attributed to the decarboxylation/oxidation reactions of remaining carbonaceous fragments from citric acid. Furthermore, the thermal treatment at 220 °C severely decomposes the metal citrate deposited on alumina surface.

Three citric acid-synthesized alumina-supported CoMo catalysts were characterized by LR spectroscopy to find out the influence of the thermal treatment over the chemical nature of Mo–oxo species deposited on alumina body. The Raman spectrum for the sample treated at 110 °C exhibits two major Raman peaks at 940 and 895 cm^{-1} together the shoulder at 860 cm^{-1} and the small bands at 372 and 210 cm^{-1} (Fig. 3), which are characteristic of the $[Mo_4O_{11}(C_6H_5O_7)_2]^{4-}$ complex, in agreement with a previous report [2]. Furthermore, the weak features at 1,075, 1,410 and ca. 1,620 cm^{-1} are associated to the C–O bond stretching and -COO^- symmetric and asymmetric stretch modes from the carboxylic groups presents in the citrate [8]. No free critic acid seems to be present considering the absent of a strong Raman peak at about 785 cm^{-1}, however, one cannot rule out a strong citrate-Al_2O_3 interaction. A strong fluorescence background was observed in the sample treated between 170 and 350 °C, probably caused by residual fragments of the organic matrix. This argument can be supported by the Raman spectrum of alumina-supported CoMo sample calcined at 400 °C, and nearly free of residual carbon, which shows strong features associated to hydrated $Mo_7O_{24}^{6-}$ anion together a shoulder at 955 cm^{-1}, likely due to nascent cobalt molybdate (β-$CoMoO_4$) phase [17, 18]. The overall analysis of the Raman spectra for alumina-supported CoMo catalyst confirms the formation of $[Mo_4(C_6H_5O_7)_2O_{11}]^{4-}$ complex, whilst no evidence of Co citrate complex was obtained. This finding rationalizes the strong effect of (poly)molybdate species on mitigating the violent exothermic combustion reaction of the Co + CA/Al_2O_3 sample.

After treating the γ-Al_2O_3-supported CoMo catalysts synthesized with and without citric acid at 110 and 350 °C,

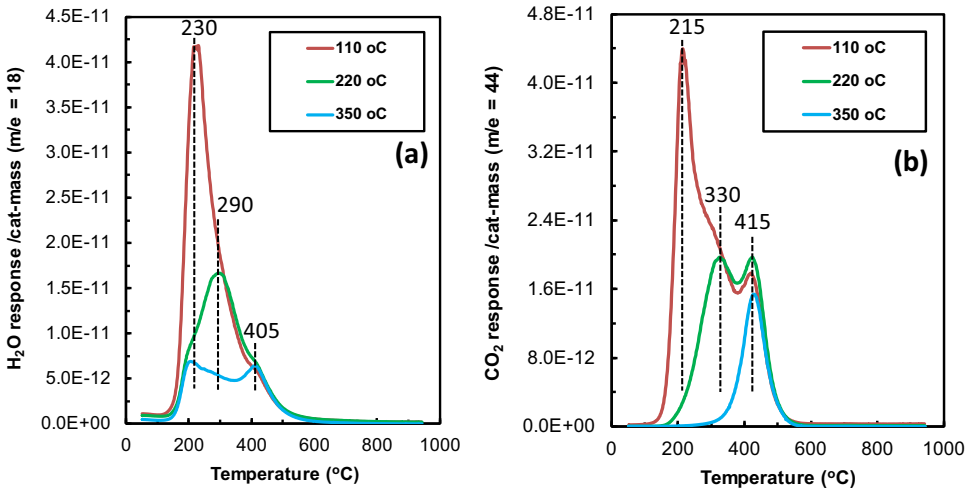

Fig. 2 TPO-MS profiles of the evolution of H_2O (**a**) and CO_2 (**b**) from citric acid-containing alumina-supported CoMo catalysts treated at different temperatures

the solid samples were characterized by powder X-ray diffraction (Fig. 4). The XRD patterns for the CA-synthesized alumina-supported CoMo catalysts do not exhibit diffraction peaks attributable to any Co and Mo–oxo species (Fig. 4a). Indeed, only γ-alumina diffraction peaks were detected (PDF No. 48–367) based on the PDF-ICDD database crystalline materials [23] as was also determined for Mo citrate on alumina [2], indicating that small domain size of Co- and Mo-oxo entities are present even after the thermal treatment at 350 °C. The strong background signal could be arisen either from the Co-based fluorescence or from the amorphous background of the alumina body.

It is worth remarking that no crystallite mixed-metal oxides (i.e., $Al_2(MoO_4)_3$, $CoMoO_4$, $Co_2Al_2O_4$) were observed. On the other hand, the XRD analysis for the equivalent CoMo catalyst synthesized without citric acid showed not only the γ-alumina diffraction peaks but also partially hydrated cobalt nitrate (PDF No. 18-424) peaks in the sample treated at 110 °C (Fig. 4b). After treating the CoMo formulation at 350 °C, the main diffraction peak of cobalt molybdate (β-$CoMoO_4$) at ca. 26° in 2θ (PDF No. 21–868) together the γ-alumina are displayed, in agreement with a previous report [17]. This finding clearly reveals that the presence of citric acid upon the synthesis of alumina-supported CoMo catalyst leads to the formation of poorly crystallized or well-dispersed Co and Mo citrate species in the sample treated at low thermal treatment (i.e., 110 °C). These amorphous or nano-dispersed species hinder the formation of mixed-metal oxides (i.e., $CoMoO_4$ and likely $CoAl_2O_4$) and could enhance the formation of small domain size of Co- and Mo-oxo species upon the treatment of CoMo formulation at high temperature (i.e., 350 °C). Thus, citric acid clearly prevents the aggregation of the metal component particles during the calcinations process.

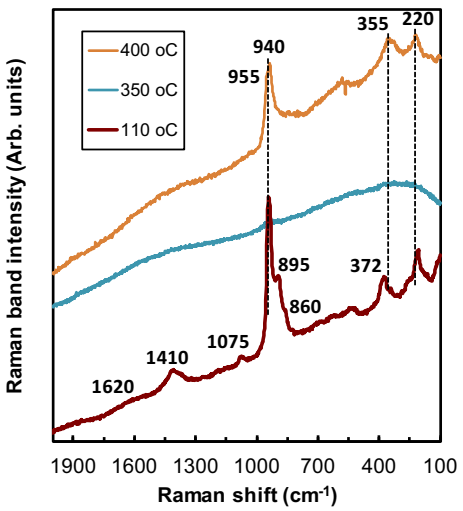

Fig. 3 Laser Raman spectra of the citric acid-containing alumina-supported CoMo catalysts treated at various temperatures

Figure 5a exhibits an abrupt increase of the specific surface area and a reduction of the bulk density relative to the sample treated at 110 °C when the citrate-containing CoMo catalyst is thermally treated at 220 °C. Indeed, citric acid-synthesized CoMo catalyst treated at 220 °C showed a 3.7-fold increase of surface area relative to the 110 °C-treated sample, on the other hand, the CoMo catalyst bulk density dropped by 16 %. Calcination temperatures below 170 °C and above 220 °C did not affect severally the specific surface area and bulk density compared to the CoMo catalysts treated at 110 and 350 °C, respectively. The severe increase of the specific surface area and diminution of the bulk density is a consequence of the decomposition of Co and Mo citrate on alumina as was confirmed by TGA–DSC and TPO–MS analysis. This trend was also reflected in the variation of the pore volume distribution with the thermal treatment (Fig. 5b). That is, the BJH desorption curves for the CoMo catalysts treated at 110 and 170 °C show a single modal pore distribution centred at approximately, 130 Å, whilst the thermal treatment at temperatures above 220 °C leads to a bimodal pore distribution. This narrow porous distribution was also observed in low loadings of Co (1–3 %) and Mo (4–11 %) sulfide on γ-alumina synthesized with citric acid as chelating agent [28]. It is worth remarking that the new narrow pore system centred at 60 Å for 220 °C-treated sample is slightly shifted to higher pore diameter (i.e., from 60 to 75 Å) as increasing the calcination temperature. Note, however, that the maximum position of the high pore diameter peak (ca. 130 Å) does not appear to vary significantly with thermal treatment. The evolution of the bimodal pore distribution with the treatment temperature would indicate that Co cations and Mo citrate are mainly deposited onto the mesoporous of γ-alumina with diameter below 90 Å. In addition, the generation of some porosity after treatment at 400 °C suggests that residual carbonaceous material still remains in the CoMo catalyst calcined at 350 °C, in agreement with the TGA–DSC and TPO–MS analysis. Furthermore, its SSA based on alumina loading was 20 % lower than that for γ-alumina because of residual organic matrix and/or partial collapse of alumina mesoporosity.

Characterization of citric acid-containing γ-alumina-supported CoMo catalysts by TPR-MS and HRTEM

The analysis of the evolved and consumed gases upon the temperature-programmed reduction of the citric acid-containing alumina-supported Co, Mo and CoMo catalysts can give further insight into the thermal decomposition of the metal citrate species under reducing conditions and also the possible interaction between the catalyst components (i.e., Co, Mo and Al_2O_3). Two major reduction processes denoted low-temperature (LT) and high-temperature (HT)

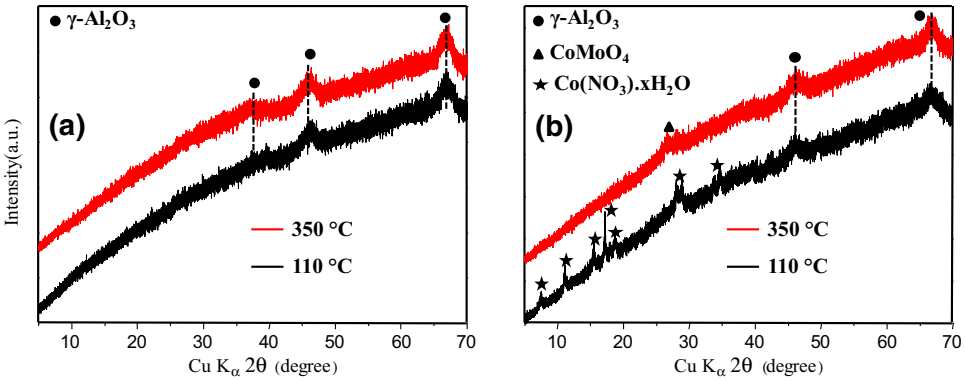

Fig. 4 Powder XRD patters for CoMo + CA/γ-Al_2O_3 (**a**) and Co nitrate + AHM/γ-Al_2O_3 catalysts (**b**) treated at 110 and 350 °C

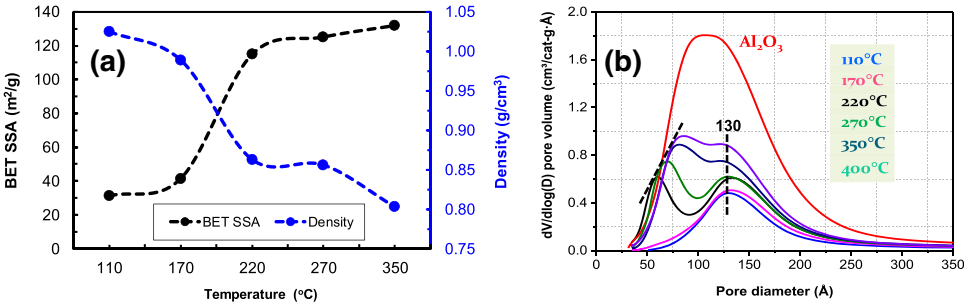

Fig. 5 Dependence of the BET specific surface area (SSA), bulk density (**a**) and pore volume distribution (**b**) with the thermal treatment of citric acid-synthesized Al_2O_3-supported CoMo catalysts

peaks are clearly displayed in the Mo and CoMo formulations, Fig. 6a.

The LT peak is associated with the likely partial reduction of polymolybdate from Mo^{6+} to Mo^{4+} and the HT reduction peak is assigned to the subsequent reduction of polymolybdate-partially reduced entities and monomeric tetrahedrally coordinated Mo species [17, 29]. Comparison of the TPR–MS profiles of the monometallic samples (i.e., Co and Mo) with the bimetallic catalysts (i.e., CoMo) suggests that a major fraction of Co species are also reduced at the LT peak. Apparently, Mo and Co species are also taken part in the small hydrogen consumption peaks at 205 and 595 °C, respectively. Note that the intensity of the former peak decreased and the maximum of the latter (i.e., 595 °C) was shifted to lower temperatures as increasing the thermal treatment because of the metal citrate decomposition. Note a clear shift of the maximum for the LT peak to higher reduction temperatures (i.e., from 425 to 465 °C), whilst the maximum of the HT peak is shifted toward lower temperatures (i.e., from 835 to 750 °C) when rising the catalyst thermal treatment. Furthermore, the LT peak became narrow while the HT peak is wider as increasing the treatment temperature. The HT reduction peak is ca. two-fold more sensitive to the catalyst thermal treatment that the maximum temperature for LT peak, as a consequence of the different types of species reduced in each stage. Indeed, Co^{2+} species is most likely reduced to Co metal at low temperature together a partial reduction of Mo citrate, which is subsequently reduced at HT peak. It is envisaged that cobalt could auto-catalyze the subsequent reduction of partially reduced Mo–oxo species, shifting the HT peak to lower temperatures. It is noticeable that the area of the HT reduction peak relative to the curve area of the LT peak significantly increased at treatment temperature of 220 °C and above, see inset in Fig. 6a, likely due to the severe decomposition of Co and Mo citrate species. This could increase the interaction between the metal oxides and hence facilitating an enrichment of monomeric molybdate species.

On the other hand, the evolution of water upon the temperature-programmed reduction of the citrate-containing CoMo catalysts treated at different temperatures confirms the reduction of the Co^{2+} to Co metal and Mo^{6+} to Mo^{n+} (n = 2-0) through the LT and HT peaks, Fig. 6b. Note, however, that the major evolved water peak for the samples treated up to 220 °C appears at ca. 200 °C, a marked contrast with the equivalent peak for the H_2 consumption profile. This finding can be attributed to the contribution of the dehydration and dehydroxylation reactions of citric acid and alumina, respectively. Also note that no water peak at ca. 600 °C in opposition to the H_2 consumption peak at 595 °C, which would support the assignment of this small feature to the hydrogenation of residual carbonaceous material by Co metal to produce light gas molecules as was confirmed by evolved methane and it is illustrated in Eq. (1).

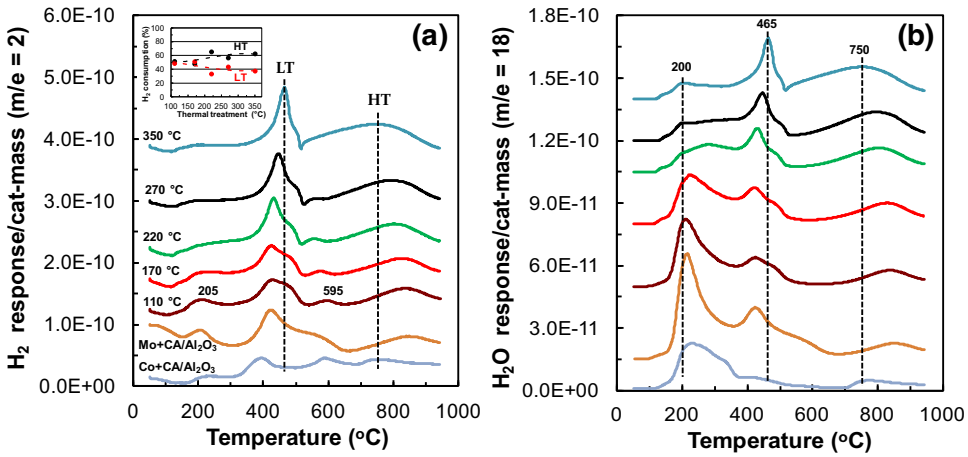

Fig. 6 TPR-MS profiles of H_2 (**a**) and H_2O (**b**) for citric acid-synthesized Al_2O_3-supported Co, Mo and CoMo catalysts. Inset: Relative H_2 consumption for low temperature (*LT*) and high temperature (*HT*) reduction peaks

$$nC + xH_2 \rightarrow C_nH_{2x} \quad (1)$$

According to the reduction peak positions, the relative hydrogen consumption and the water evolution profiles, one can conclude that the treatment temperature affects the interaction between Co and Mo species and even alumina and hence the relative concentration of reducible species. Indeed, a calcination temperature sufficient high to decompose the Mo-citrate complex (i.e., 220 °C) enhanced the Co-Mo-alumina interaction, which is reflected in a wide distribution of Mo-oxo species and relative high concentration of species reducible at HT peak. Furthermore, the dehydration of citric acid, dehydroxylation of alumina and the hydrogenation of residual carbonaceous material also take place upon the reduction process and most likely the sulfidation of the citric acid-containing CoMo catalysts.

Upon the temperature-programmed reduction analysis for the citric acid-containing CoMo catalysts it was also followed the evolution of CO_2 and CO as given in Fig. 7. Two major CO_2 peaks centred at 210 and 330 °C markedly decreased as increasing the treatment temperature to evolve a relative small amount of CO_2 at temperatures above the maximum calcination temperature (i.e., 350 °C), Fig. 7a. Indeed, the relative amount of evolved CO_2 with the treatment temperature drastically decreased in the sample calcined at 220 °C (inset in Fig. 7a) and above, this finding clearly confirms that the Mo citrate undergoes a severe process of decomposition at this temperature.

On the other hand, the evolved CO profiles showed a marked contrast to the CO_2 evolution profiles despite producing CO fragment when subjected to electron impact ionization (Fig. 7b). Indeed, the CO evolution at temperatures below 500 °C fits fairly well with the CO_2 profile as was verified by following the evolution of carbon (m/e = 12). However, the strong CO peak centred at 525 °C does not have an equivalent one in the evolved CO_2 profiles. This discrepancy is tentatively rationalized by the partial oxidation of residual carbonaceous material to produce carbon monoxide and hydrogen, Eq. (2).

$$C + H_2O \rightarrow CO + H_2 \quad (2)$$

It is envisaged that part of the water produced by either the reduction of Co cation and Mo citrate in the LT reduction step or even the dehydroxylation of alumina could participate in this reaction, which could be catalyzed by partially reduced CoMo (or even $CoMoOC_x$) species [10, 30]. It should be mentioned that a strong peak at 525 °C from apparently H_2 (and CO) production was observed in the TCD response (result not shown); however, H_2 was not clearly discernible in the MS response, likely due to the rapid H_2 consumption by the subsequent reduction reactions. It is noticeable a strong diminution of the overall evolved CO in the CoMo catalysts treated at temperatures above 220 °C compared to the samples treated at lower temperatures as a consequence of its relatively lower content of residual carbon, see inset in Fig. 7b.

The evolution of CO and CO_2 was also monitored in the citric acid-containing alumina-supported Co and Mo samples to find out the potential effect of Co and Mo over the evolved CO in the TPR–MS profiles (Fig. 8).

The Mo-containing catalysts and even CA deposited on alumina exhibit a major evolved CO_2 peak at 205 °C, whilst the alumina-supported Co citrate sample underwent a major decomposition step at 350 °C, Fig. 8a. Note that the bimetallic CoMo formulation and the CA/Al_2O_3 also showed a peak at about 350 °C. These maximum temperatures are comparable to the maximum obtained by TGA, particularly for Mo + CA/Al_2O_3 and CoMo + CA/Al_2O_3 samples; see Fig. 1b, despite the different atmospheres (i.e., dried air vs. 10 % H_2 in Ar). On the other hand, the Mo + CA/Al_2O_3 showed a very strong CO peak at 645 °C that coincides with an apparent hydrogen production peak (see Fig. 6a). This CO peak is shifted to lower temperature (i.e., 525 °C) in the CO profile of CoMo + CA/Al_2O_3 catalyst (Fig. 8b). This finding clearly illustrates a

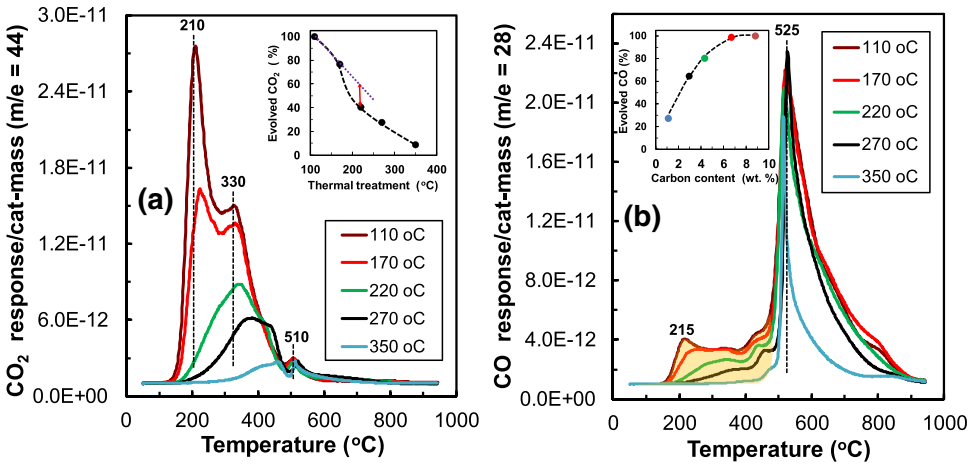

Fig. 7 TPR-MS profiles of CO_2 (**a**) and CO (**b**) for citric acid-synthesized Al_2O_3-supported CoMo catalysts. Insets: Dependence of the evolved CO_2 with the thermal treatment (**a**) and evolution of CO with carbon content (**b**)

positive effect of the bimetallic CoMo formulation relative to the monometallic Mo sample over the CO evolution though the Eq. 2, likely due to the effective Co-Mo interaction. Furthermore, the evolution of CO during the temperature-programmed reduction of citric acid-containing Co(or Ni)Mo catalyst could be a valuable approach to elucidate the potential interaction (or promoter effect) between Co (or Ni) and Mo-xo species under reducing conditions.

A summary of the different reactions involved upon the reducing treatment in 10 % H_2 in Ar of the citric acid-synthesized CoMo catalyst is given in Fig. 9. Note that only decomposition reactions take place at temperatures below 350 °C, whilst the reduction reaction of Co–Mo species, gasification and hydrogenation of residual carbonaceous material occurred at temperatures higher than 400 °C. It is worth mentioning that Co metal or even $CoMoOC_x$ may catalyze the reduction reactions at temperatures above 600 °C.

Representative HRTEM images in different nano-scale of γ-alumina-supported CoMo sulfide catalyst are shown in Fig. 10. A schematic representation of the evolution of Co and Mo citrate species with the thermal treatment to produce Co and Mo–oxo species dispersed on alumina and the panoramic image of the sulfided catalyst is given in Fig. 10a. Molybdenum sulfide (i.e., 2H-MoS_2 stacking) consists of slabs, each of which comprises a plane of Mo atoms sandwiched between two hexagonal close-packed planes of sulfur atoms. A panoramic view reveals the dispersion of layered structures on alumina surface (Fig. 10a). The micrographs display mainly the edge or prism planes with layer stacking spacing of ca. 6.1 Å characteristic of MoS_2 [32]. The slabs are partially intercalated by another slab and are bent on a longer scale to maximize the interaction with the alumina surface (Fig. 10b). The interaction of Co sulfide with MoS_2 would lead to the formation of local active type II Co–Mo–S structures [20, 43], taking into account the stacking layers displayed in Fig. 10b.

Dependence of the catalytic performance of citric acid-containing γ-alumina-supported CoMo with the thermal treatment

To find out the effect of the impregnation time over the HDS activity of citric acid-containing CoMo catalyst using

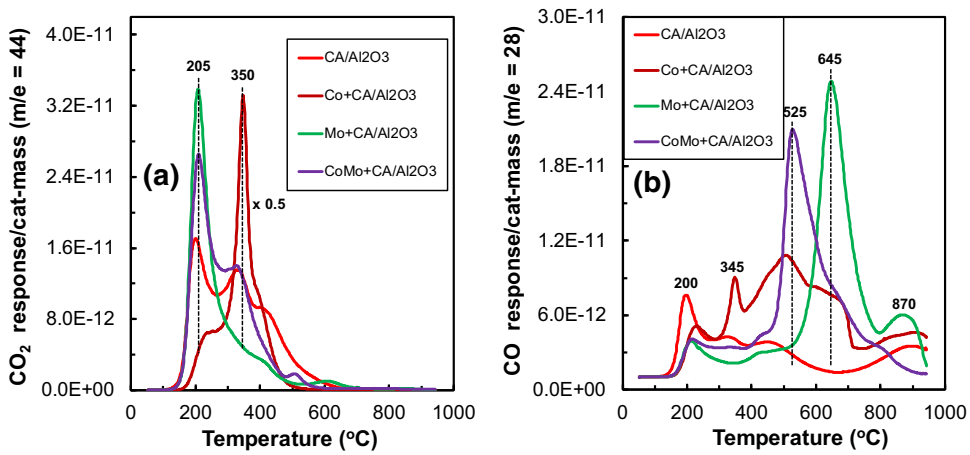

Fig. 8 TPR-MS profiles of CO_2 (**a**) and CO (**b**) for citric acid-containing alumina-supported Co, Mo and CoMo catalysts

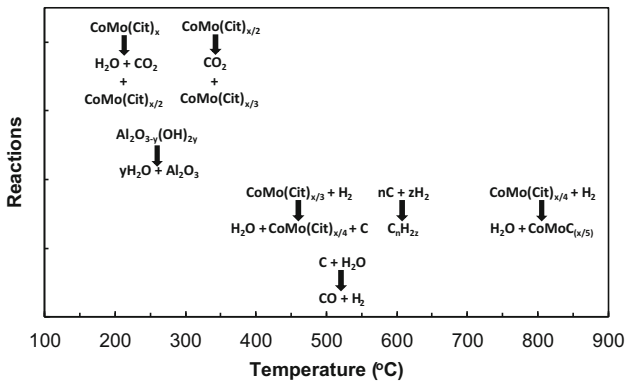

Fig. 9 Tentative schematic representation of the different reactions involved in the temperature-programmed reduction of γ-alumina-supported Co and Mo citrate catalyst. $CoMo(Cit)_x$ complex represents the Co and Mo citrate precursor deposited on γ-alumina, whose degradation with the reduction temperature is given by $CoMo(Cit)_{x/n}$ ($n = 2$–4)

feed 2 as feedstock, a series of samples prepared by wet impregnation were catalytically examined. It is worth pointing out that the HDS rate constants were calculated with the law kinetic expression (Eq. 3) given below:

$$\frac{1}{S_P^{n-1}} - \frac{1}{S_F^{n-1}} = \left(\frac{n-1}{\text{LHSV}}\right) k_{\text{HDS}} \tag{3}$$

Where S_F is the sulfur concentration in the feedstock (μg S g^{-1} sample), S_P is the sulfur concentration in the product (μg S g^{-1} sample), n is the apparent reaction order, which was assumed to be of 1.5 based on a previous work [15]. The LHSV is the liquid hourly space–velocity (min^{-1}) and k_{HDS} corresponds to the overall HDS reaction constant [$1/cm^3$ s $wppm^{(n-1)}$].

Figure 11 clearly illustrates that the impregnation period longer than 4 h did not affect markedly the HDS rate constant, a similar trend was observed in the dependence of the catalyst density with impregnation time. This finding suggest that after ca. 4 h of impregnation a maximum loading of Co, Mo and citric acid was adsorbed/deposited on extruded alumina body. Taking into account this finding, the subsequent CoMo catalysts were synthesized using an impregnation time between 5 and 24 h.

Figure 12 compares the residual sulfur content in the liquid products obtained from the hydrotreatment of two different feeds over alumina-supported CoMo sulfide catalysts treated at different temperatures. It is noticeable that the remaining sulfur concentration in the hydro-treated product slightly increased with the severity of the catalyst thermal treatment because of the decomposition of the metal precursors (Co and Mo citrate) deposited on alumina. Also note that the residual sulfur contents from feed 1 are markedly lower than those obtained from feed 2, indicating that the former feed (mode feed) is less demanding that the latter feed (real feed).

The HDS and HDN rate constants for various alumina-supported CoMo sulfide catalysts over feed 1 and feed 2 are listed in Table 3. The overall HDN rate constant was determined using a first order kinetic equation (Eq. 4):

$$\ln\left(\frac{N_F}{N_P}\right) = k_{\text{HDN}}\left(\frac{1}{\text{LHSV}}\right) \tag{4}$$

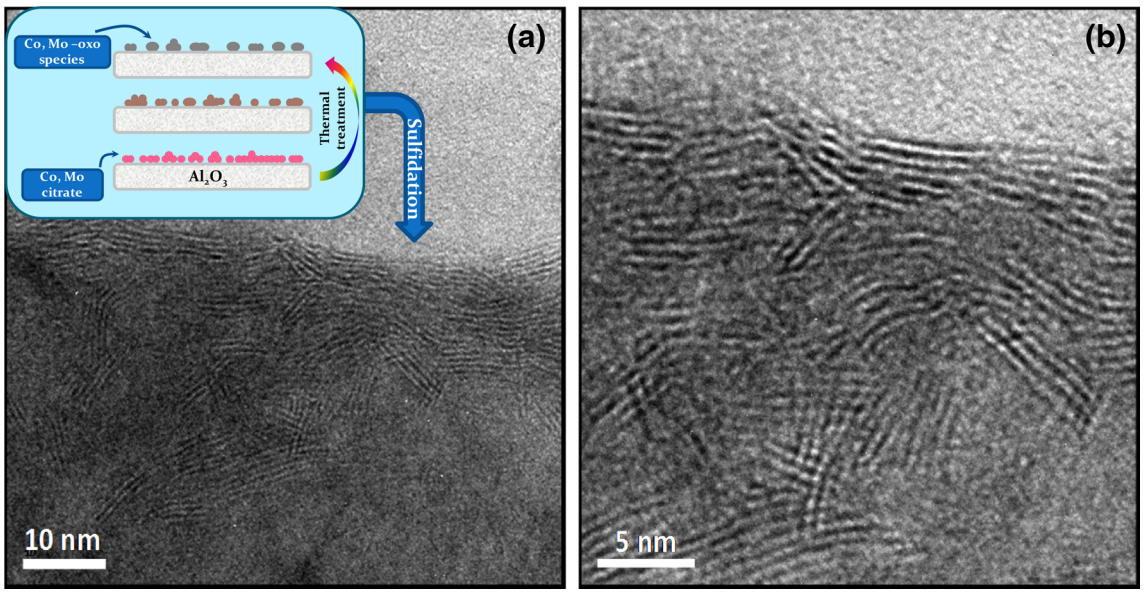

Fig. 10 HRTEM images of 110 °C-treated citric acid-synthesized alumina-supported CoMo sulfide catalyst: panoramic view (**a**) and magnified image (**b**)

N_F is the nitrogen concentration in the feedstock (μg N g^{-1} sample), N_P is the nitrogen concentration in the product (μg N g^{-1} sample) and k_{HDN} corresponds to the overall HDN reaction constant (1/cm^3 s).

It is worth mentioning that an apparent reaction order of 1.3 (feed 1) and 1.5 (feed 2) for the HDS reactions and 1.0 for HDN reactions were assumed, taking into account a previous report [15, 16]. Note that both feeds show a slightly inverse dependence of the HDS activities with the catalyst thermal treatment. This trend is attributed to the decomposition of the Co^{2+} and Mo^{6+} citrate upon the thermal treatment that markedly attenuates the Co-promoter effect over Mo species. It is a consequence of the possible formation of poorly reducible mixed-metal oxides as is inferred by H_2-TPR-MS, laser Raman spectroscopy and X-ray diffraction analysis. On the other hand, the citric acid-synthesized CoMo formulation by sequential impregnation (i.e., first Mo citrate solution was deposited on alumina and treated at 275 °C and then it was impregnated with Co citrate solution and dried at 110 °C) showed clearly lower HDS activity than the CoMo catalysts prepared by wet co-impregnation, see Table 3. However, the citric acid-synthesized CoMo formulations were significantly more active than the commercial alumina-supported CoMo catalyst.

This finding evidences that citric acid plays a major role in the effectiveness of the Co–Mo interaction that would be reflected in an efficient Co promoter effect and enhanced HDS activity [6]. Note that the HDS and HDN activities from feed 1 were noticeable higher than those obtained from feed 2, suggesting that the former feed is clearly more reactive (or less demanding) than the later (i.e., feed 2) based on the reactivity of S and N compounds. Indeed, the trend obtained for these two feeds suggests that feed with higher apparent HDS reaction order, lower density and even higher end-boiling point is less reactive, as a consequence of the higher concentration of S-containing compounds (see Table 1) in agreement with a previous work [16]. Hence, more demanding conditions of reaction are required to produce ultra-low sulfur fuel.

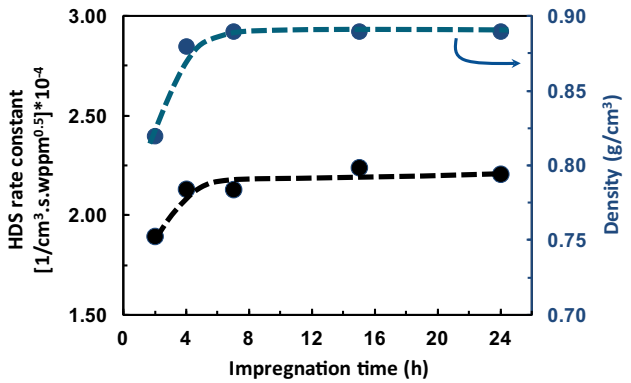

Fig. 11 Dependence of HDS rate constant on the impregnation time for alumina-supported CoMo sulfide catalysts synthesized by wet impregnation with citric acid-containing Co-Mo solution. Catalytic reactions conducted at 340 °C, 3.5 MPa, 250 Nm^3/m^3 (H_2/Oil ratio) and 7.2 h^{-1} using feed 2 as feedstock

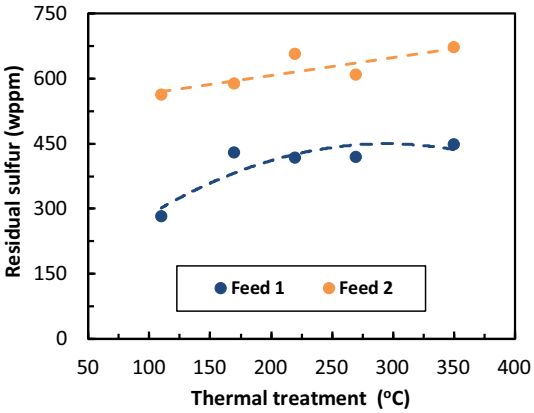

Fig. 12 Influence of the catalyst thermal treatment over the residual sulfur content in the citric acid-synthesized alumina-supported CoMo sulfide catalysts over two different feeds. Catalytic reactions conducted at 340 °C, 3.5 MPa, 250 Nm^3/m^3 (H_2/Oil ratio) and 7.2 h^{-1}

It is also noticeable a clear improvement, particularly in the HDS and HDN activities over feed 1, for the citric acid-synthesized CoMo catalysts compared to the commercial CoMo catalyst, Table 3. This finding suggests that the use of citric acid to synthesize the CoMo formulations enhances not only the C–S bond scission through the direct desulfurization pathway, but also the hydrogenation route [14, 42], which is the main catalytic pathway for the HDN reactions and also for refractory S-containing organic compounds on NiMo(W) catalysts [16].

To illustrate the influence of the Mo citrate degradation over the HDS activity it was plotted the remaining carbon content in the thermally treated CoMo catalyst versus the HDS activity. A relatively linear dependence of the catalyst activity with the residual carbon is displayed in Fig. 13 suggesting that the gradual degradation of the whole metal citrate has a detrimental effect over the HDS activity, likely due to the strong Co–Mo–alumina interactions. Again, HDS activity from feed 1 was significantly higher than that obtained from feed 2. Note that the lineal dependence given in Fig. 13 corresponds to CoMo catalyst precursor rather than the CoMo sulfide, indicating that the genesis of the catalyst preparation from the aqueous solution would play a major role in the definition of the catalyst activity under the sulfidation condition used in this work. It should be pointed out that the remaining carbon in the citric acid-synthesized CoMo catalyst precursors treated at different temperatures could not be necessary the residual carbon in the CoMo sulfide catalyst after the sulfidation process, since Mo citrate would be largely decomposed based on the

Table 3 HDS and HDN rate constants for citric acid-synthesized alumina-supported CoMo sulfide catalyst treated at different temperatures and commercial CoMo sulfide catalyst over feed 1 and feed 2. Catalytic reactions carried out at 340 °C, 3.5 MPa, 250 Nm^3/m^3 (H_2/Oil ratio) and 7.2 h^{-1} (LHSV)

Feedstock reaction reaction order catalyst	Feed 1 HDS 1.3 k(1/cm^3 s $wppm^{0.3}$)*10^{-4}	Feed 2 HDS 1.5 k(1/cm^3 s $wppm^{0.5}$)*10^{-4}	Feed 1 HDN 1.0 k(1/s.cm^3)	Feed 2 HDN 1.0 k(1/s.cm^3)
110	13.8	2.2	28.1	5.9
220	11.1	1.9	23.2	6.8
270	11.1	2.0	22.3	6.5
350	10.7	1.9	20.6	5.9
Mo cit @275̊C & Co cit @110̊C	10.1	1.8	20.3	5.9
Commercial CoMo	7.4	1.3	17.5	5.9

evolution of CO_2 under reducing conditions (i.e., TPR-MS analysis) and the relatively low amount of residual carbon after calcination at 350 °C (i.e., 1.1 wt. %) under oxidizing atmosphere. Therefore, the main role of the citric acid upon the synthesis of alumina-supported CoMo catalyst would be the generation of poorly crystallized or well-dispersed Co and Mo citrate species at low thermal treatment (i.e., 110 °C). These amorphous and nano-dispersed species hinder the formation of (bulk) mixed-metal oxides and could enhance the formation of type II CoMoS structure upon the sulfidation process. This type II structure has weaker interaction with the support and higher intrinsic activity than type I active phase [20]. Nevertheless, we cannot rule out a possible effect of the residual carbon on the morphology of the type II CoMoS structure and thereby the catalyst performance [34].

A comparative study of the dependence of the residual sulfur content in the hydro-treated product with operation time for alumina-supported CoMo sulfide catalysts under deep hydrotreating conditions is given in Fig. 14. The relatively lower sulfur concentration (ca. 90 wppm) in the obtained liquid product from the citric acid-synthesized CoMo sulfide catalyst compared to that obtained from commercial CoMo sulfide catalyst (ca. 125 wppm) in the apparent steady state clearly illustrates the positive effect of citric acid-based synthesis over the HDS activity.

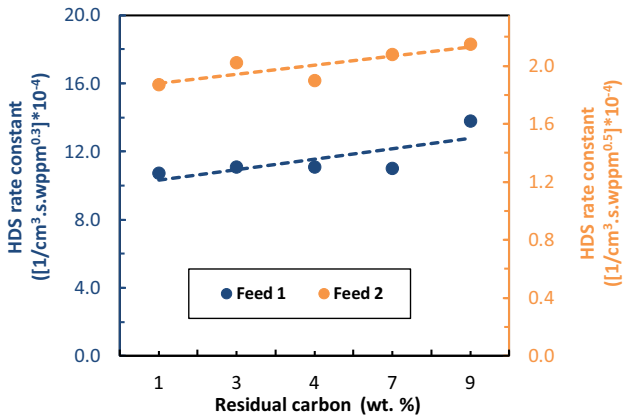

Fig. 13 Dependence of the HDS rate constant with the residual carbon content for citric acid-synthesized alumina-supported CoMo sulfide catalysts. Reactions carried out at 340 °C, 3.5 MPa, 250 Nm^3/m^3 (H_2/Oil ratio) and 7.2 h^{-1} (LHSV)

Indeed, the increase of the reaction temperature up to 350 °C enhances not only the concentration of residual sulfur to ca. 40 wppm, but also the cetane index of the hydro-treated product compared to the feedstock (i.e., from 45.2 to around 65 units), see inset in Fig. 14, likely due to the partial hydrogenation of poly-aromatic compounds [16]. An increase of approximately, 40 % of the residual sulfur content in the hydro-treated product at time on stream below 100 h exhibited the citric acid-synthesized CoMo sulfide formulation because of catalyst deactivation. This is a consequence of the very high reactivity of CoMoS nano-structure highly-dispersed on alumina surface. It has been found in this work that the use of citric acid enhances the catalyst activity compared to the commercial CoMo catalyst even after treating the catalyst precursor at high temperature, which could improve the catalyst stability and still exhibit a relatively high HDS activity.

Solution chemistry of Co and Mo citrate and its role upon adsorption-deposition on alumina

It is currently well-established that the stoichiometric ratios of Mo to citrate (2:1, 1:1, 1:2) are strongly dependent upon solution pH (Cruywagen and Van de Water [7]. A similar effect has been also determined for Co-citrate complex [3], which was observed at pH 5 and 9 as at pH 1 only $[Co(H_2O)_6]^{2+}$ and citric acid were detected. Unfortunately, a similar study for Co and Mo citrate-containing solution is not currently available. Nevertheless, a recent report revealed that a bimetallic CoMo citrate complex could be present in aqueous solution when pH is between 1.5 and 3.5, according to ^{17}O and ^{13}C NMR results [24]. A high HDS activity for straight run gas oil of citrate-prepared CoMo catalyst was attributed to the particular composition

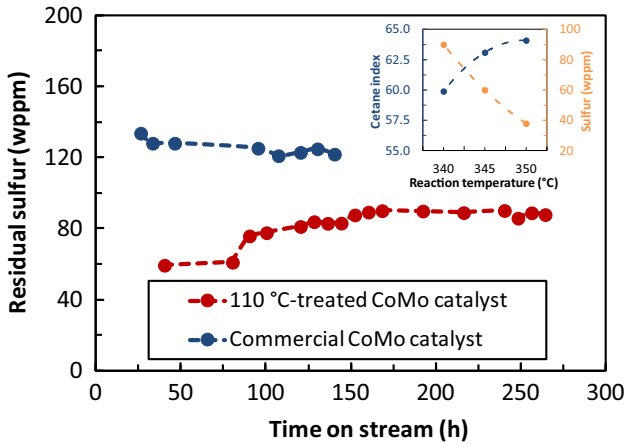

Fig. 14 Dependence of the residual sulfur content with time on stream over feed 2 for the 110 °C-treated CoMo and commercial CoMo sulfide catalysts [hydrotreating reactions conducted at 340 °C, 3.5 MPa, 250 Nm^3/m^3 (H_2/Oil ratio) and 1.2 h^{-1}]. *Inset* Effect of the reaction temperature over the cetane index and residual sulfur content in the hydro-treated product

(Co/Mo = 0.5) and stability of the CoMo citrate complex [37]. However, according to Fujikawa the enhanced hydrotreating performance of citrate-prepared CoMoP formulation is due to the chelating effect of citrate on cobalt that preventing its sulfidation at low temperatures [11, 12], facilitating the interaction of Co sulfide with MoS_2-like structure and hence the synergy between Mo and Co. Furthermore, the decomposition of the Co complex upon the sulfidation temperature is limited by kinetic factors thereby the chelating agent can adjust timing when Co ions interact with the MoS_2-like structure [35].

Protonation and deprotonation of the surface hydroxyl groups are the common reactions when alumina is wetted into an aqueous solution [49]. The point of zero charge (PZC) of alumina is usually between 8 and 9 pH [27]. The presence of water molecule on alumina surface increases the solution pH because of pH buffer effect (Eq. 5).

$$Al_SOH + H^+ \rightarrow Al_SOH_2^+ \quad (5)$$

When alumina is wetted into a solution of citric acid (i.e., $CitrH_4$) at low pH (below 5), citrate anion can react with alumina surface [19], causing a highly negative charged surface and a shift of the PZC to lower pH values. This interaction can take place on Lewis acid sites of alumina to release a molecule of water (Eq. 6).

$$CitrH^{3-} + Al_SOH_2^+ \rightarrow [Al_S - CitrH]^{2-} + H_2O \quad (6)$$

Upon the synthesis of alumina-supported CoMo catalysts by wet impregnation the formation of $Co_2[Mo_4O_{11}(CitrH)_2]\cdot H_2O$ should be taken into account [24]. Also the presence of Mo citrate (or ammonium Mo citrate) and $[Co(H_2O)_6]^{2+}$ complexes in aqueous solution (Eq. 7) should be taken into consideration.

$$[Co(H_2O)_6]_2[Mo_4O_{11}(CitrH)_2] \rightarrow [Mo_4O_{11}(CitrH)_2]^{4-} + 2[Co(H_2O)_6]^{2+} \quad (7)$$

According to the CoMo catalyst synthesis employed in this work, a CA/Mo molar ratio of approximately one was used as Mo citrate complex has a molar ratio of 0.50. The excess of citric acid in the aqueous solution could interact with $[Co(H_2O)_6]^{2+}$ complex and even alumina surface through the citrate ligand effect [19]. However, it was found no evidence of the partial dissolution of alumina despite the relatively high concentration of citric acid (i.e., 0.8 mol L^{-1}) and long period of impregnation (4–6 h). Nevertheless, we cannot rule out a potential interaction between alumina surface and citrate anion (Eq. 6).

The Co and Mo compositions were determined by ICP-AES, and it is shown that alumina-supported CoMo catalyst precursor prepared by wet co-impregnation and calcined at 350 °C had 23 wt. % MoO_3 and 4.7 wt. % CoO, which is fairly close to the nominal composition (i.e., 24 wt. % MoO_3 and 6 wt. % CoO). However, the MoO_3/CoO mass ratio (i.e., 4.9) is clearly larger than the nominal ratio (i.e., 4.0). This finding indicates that upon impregnation process Co^{2+}-alumina interaction is weaker than Mo^{6+}–alumina interaction, owing to the favorable electrostatic interaction of Mo^{6+} citrate species with alumina surface. The $[Co(H_2O)_6]^{2+}$ complex seems to interact preferentially with surface neutral OH groups in the formation of inner-sphere Co^{2+} surface complexes as $[Mo_4O_{11}(CitrH)_2]^{4-}$ complex prefers surface basic OH groups through electrostatic interaction. Therefore, the adsorption of these complexes can be apparently governed by the surface density of these OH groups on alumina surface, concentration and solution pH. Considering a typical value of ionizable Al–OH group of 0.5 μmol/m^2 [5] and an alumina surface area of 250 m^2 g^{-1}, a total weight loading of ca. 6 % MoO_3 on alumina would be expected. Note that it is assumed that Mo is exclusively deposited on alumina by equilibrium adsorption (i.e., no precipitation). This Mo loading is significantly lower than that deposited on alumina for the prepared CoMo catalysts, most likely due to the precipitation of Co and Mo citrate upon impregnation process. Indeed, the use of highly concentrated CoMo citrate solution [i.e., 1.28 mol L^{-1} (Mo), 0.64 mol L^{-1} (Co) and 1.28 mol L^{-1} (CA)] can be apparently destabilized by alumina body (heterogeneous nucleation), inducing the metal (hidro)oxide precipitation (i.e., alumina-assisted CoMo citrate precipitation) at long period of impregnation (above 4–5 h). It is worth remarking that nearly 80 wt. % of the Co and Mo citrate deposited on alumina can be removed by water extraction, which supports the

conclusion that most of the material loaded on alumina surface is due to the deposition–precipitation process.

Conclusions

A series of citric acid-synthesized γ-alumina-supported CoMo catalyst precursors treated at various temperatures and sulfided with middle distillate spiked with dimethyl disulfide (4 wt. % sulfur) at 350 °C was catalytically examined for deep HDS and HDN reactions over two different feedstocks. The characterization and catalytic results have been compared with an equivalent CoMo catalyst synthesized without citric acid and also a commercial γ-alumina-supported CoMo sulfide catalyst. Based on the characterization and catalyst performances, the following conclusions can be drawn:

1. The synthesis of alumina-supported CoMo catalyst precursor by wet co-impregnation using citric acid as chelating agent in the CoMo impregnation solution takes place mainly through the uniform deposition–precipitation of Co aqueous-complex and Mo citrate onto γ- alumina. It is envisaged that γ-alumina assists the precipitation of Co^{2+} and Mo^{6+} species, which cover a large fraction of mesoporous with diameter below 90 Å from the γ-Al_2O_3 carrier. This process leads to the formation of poorly crystallized but well-dispersed Co aqueous-complex and Mo citrate in the sample treated at low thermal treatment (i.e., 110 °C). These nano-dispersed metal species hinder the (bulk) formation of mixed-metal oxide (i.e., β-$CoMoO_4$) and enhance the formation of small domain size of Co- and Mo-oxo species upon the thermal treatment of CoMo formulation at high temperature (i.e., 350 °C). Indeed, citric acid mitigates the aggregation of metal component particles during calcination.
2. The decomposition reaction of Co aqueous-complex and Mo citrate deposited on alumina starts at the treatment temperature of 220 °C, facilitating the Co–Mo and Co–Mo–Al_2O_3 interactions. This is reflected in a wide distribution of Mo–oxo species. Upon the reduction process and most likely the sulfidation of the citric acid-containing CoMo catalysts also take place the dehydration and subsequent decarboxylation of citrate, dehydroxylation of alumina and the hydrogenation of residual carbonaceous material. The CO evolution upon the TPR-MS analysis from the bimetallic CoMo catalyst occurred at lower temperature than that for the Mo formulation because of the effective interaction (or promoter effect) between Co and Mo-xo species.
3. A feedstock with lower density, higher end-boiling point and high sulfur concentration (i.e., feed 2; real feed) shows lower HDS and HDN reactivity, requiring more demanding operating conditions to obtain the resulting hydrocarbon liquid product with relatively low sulfur and nitrogen contents. A maximum loading of Co and Mo citrate is deposited on alumina after 4 h of impregnation to obtain the maximum HDS activity. However, the gradual degradation of the metal citrate with increasing treatment temperature decreased the Co-promoter effect over Mo species because of the apparent formation of poorly reducible mixed-metal oxides, which have a detrimental effect over the overall catalyst activity.
4. The citric acid as chelating agent in the synthesis of CoMo formulations enhances not only the C–S bond scission through the direct desulfurization pathway, but also the hydrogenation route. The main role of the citric acid upon the synthesis of alumina-supported CoMo catalyst enters on the generation of poorly crystallized and nano-dispersed Co and Mo citrate species in the dried sample. These well-dispersed species have a weak interaction with alumina surface, which enhances the formation of type II CoMoS structure upon the sulfidation process.

Acknowledgments The authors are indebted to the KASCT-Oxford Petrochemical Research Centre for funding.

References

1. Bartholomew C, Farrauto RJ (2006) Fundamentals of industrial catalytic processes, 2nd edn. Wiley, New Jersey
2. Bergwerff J, Jansen M, Leliveld BG, Visser T, de Jong KP, Weckhuysen BM (2006) Influence of the preparation method on the hydrotreating activity of MoS2/Al2O3 extrudates: a Raman microspectroscopy study on the genesis of the active phase. J Catal 243:292–302
3. Bergwerff J, Lysova AA, Espinosa-Alonso L, Koptyug IV, Weckhuysen BM (2008) Monitoring transport phenomena of paramagnetic metal-ion complexes inside catalyst bodies with magnetic resonance imaging. Chem Eur J 14:2363–2374
4. Campanati M, Fornasari G, Vaccari A (2003) Fundamentals in the preparation of heterogeneous catalysts. Catal Today 77: 299–314
5. Carrier X, Lambert JF, Che M (1997) Ligand-promoted alumina dissolution in the preparation of MoOx/γ-Al2O3 catalysts: evidence for the formation and deposition of an Anderson-type alumino heteropolymolybdate. J Am Chem Soc 119:10137–10146
6. Castillo-Villalón P, Ramirez J, Vargas-Luciano A (2014) Analysis of the role of citric acid in the preparation of highly active HDS catalysts. J Catal 320:127–136

7. Cruywagen J, Van de Water RF (1986) Complexation between Molybdenum(VI) and citrate: a potentiometric and calorimetric investigation. Polyhedron 5:521–526
8. De Gelder J, De Gussem K, Vandenabeele P, Moens L (2007) Reference database of Raman spectra of biological molecules. J Raman Spectrosc 38:1133–1147
9. DeBoer J, Fortuin JMH, Lippens BC, Meijs WH (1963) Study of the nature of surfaces with polar molecules II. The adsorption of water on aluminas. J Catal 2:1–7
10. Encinar J, González JF, Sabio E, Rodríguez JJ (2000) Catalyzed gasification of active carbon by oxygen: influence of catalyst type, temperature, oxygen partial pressure and particle size. J Chem Technol Biotechnol 75:213–222
11. Fujikawa T (2009) Highly active HDS catalyst for producing ultra-low sulfur diesel fuels. Top Catal 52:872–879
12. Fujikawa T, Kimura H, Kiriyama K, Hagiwara K (2006) Development of ultra-deep HDS catalyst for production of clean diesel fuels. Catal Today 111:188–193
13. Geus K (2007) Production of supported catalysts by impregnation and (viscous) drying. In: Regalbuto J (ed) Catalyst preparation science and engineering. CRC Press, London, pp 341–372
14. González-Cortés S (2009) Comparing the hydrodesulfurization reaction of thiophene on γ-Al2O3 supported CoMo, NiMo and NiW sulfide catalysts. React Kinet Catal Lett 97:131–139
15. González-Cortés S, Rodulfo-Baechler SR, Imbert FE (2014a) Solution combustion method: a convenient approach for preparing Ni promoted Mo and MoW sulphide hydrotreating catalysts. In: Grier JM (ed) Combustion. pp 269–288
16. González-Cortés S, Rugmini S, Xiao T, Green MLH, Rodulfo-Baechler SR, Imbert FE (2014) Deep hydrotreating of different feedstocks over a highly active Al2O3-supported NiMoW sulfide catalyst. Appl Catal A Gen 475:270–281
17. González-Cortés S, Xiao T, Costa PMFJ, Fontal B, Green MLH (2004) Urea–organic matrix method: an alternative approach to prepare Co–MoS2/γ-Al2O3 HDS catalyst. Appl Catal A Gen 270:209–222
18. González-Cortés S, Xiao T, Lin T, Green MLH (2006) Influence of double promotion on HDS catalysts prepared by urea-matrix combustion synthesis. Appl Catal A Gen 302:264–273
19. Hidbert P, Graule TJ, Gauckler LJ (1996) Citric acid-A dispersant for aqueous alumina suspensions. J Am Ceram Soc 79:1857–1867
20. Hinnemann B, Nørskov JK, Topsøe H (2005) A density functional study of the chemical differences between type I and II MoS2-based structures in hydrotreating catalysts. J Phys Chem B 109:2245–2253
21. Hiroshima K, Mochizuki T, Honma T, Shimizu T, Yamada M (1997) High HDS activity of Co-Mo/Al2O3 modified by some chelates and their surface fine structures. Appl Surf Sci 121(122):433–436
22. Inamura K, Uchikawa K, Matsuda S, Akai Y (1997) Preparation of active HDS catalysts by controlling the dispersion of active species. Appl Surf Sci 121/122:468–475
23. JCPDS Powder Diffraction File (1989) International centre for diffraction data. Swarthmore, PA
24. Klimov O, Pashigreva AV, Fedotov MA, Kochubey DI, Chesalov YA, Bukhtiyarova GA, Noskov AS (2010) Co-Mo catalysts for ultra deep-HDS of diesel fuels prepared via synthesis of bimetallic surface compounds. J Molec Catal A Chem 322:80–89
25. Klimova T, Valencia D, Mendoza-Nieto JA, Hernández-Hipólito P (2013) Behavior of NiMo/SBA-15 catalysts prepared with citric acid in simultaneous hydrodesulfurization of dibenzothiophene and 4,6-dimethyldibenzothiophene. J Catal 304:29–46
26. Knözinger H, Ratnasamy P (1978) Catalytic Aluminas: surface Models and Characterization of Surface Sites. Catal Rev-Sci Eng 17:31–70
27. Kosmulski M (2002) The pH-dependent surface charging and the points of zero charge. J Colloid Interface Sci 253:77–87
28. Leonova K, Klimov OV, Gerasimov EY, Dik PP, Pereyma VY, Budukva SV, Noskov AS (2013) Textural characteristics of sulphided hydrotreatment catalysts prepared using Co–Mo complex compounds. Adsorption 19:723–731
29. López Cordero R, López Agudo A (2000) Effect of water extraction on the surface properties of Mo/Al2O3 and NiMo/Al2O3 hydrotreating catalysts. Appl Catal A Gen 202:23–35
30. Lu M, Xiong Z, Lv P, Yuan Z, Guo H, Chen Y (2013) Catalytic purification of raw gas from biomass gasification on Mo–Ni–Co/Cordierite monolithic catalyst. Energy Fuels 27:2099–2106
31. Marceau E, Carrier X, Che M (2009) Impregnation and drying. In: de Jong K (ed) Synthesis of solid catalysts. Wiley, Weinheim, pp 59–82
32. Najmaei S, Liu Z, Zhou W, Zou X, Shi G, Lei S, Yakobson BI, Idrobo J-C, Ajayan PM, Lou J (2013) Vapour phase growth and grain boundary structure of molybdenum disulphide atomic layers. Nature 12:754–759
33. Nikulshin P, Ishutenko DI, Mozhaev AA, Maslakov KI, Pimerzin AA (2014) Effects of composition and morphology of active phase of CoMo/Al2O3 catalysts prepared using Co2Mo10–heteropolyacid and chelating agents on their catalytic properties in HDS and HYD reactions. J Catal 312:152–169
34. Nikulshin P, Tomina NN, Pimerzin AA, Kucherov AV, Kogan VM (2010) Investigation into the effect of the intermediate carbon carrier on the catalytic activity of the HDS catalysts prepared using heteropolycompounds. Catal Today 149:82–90
35. Ohta Y, Shimizu T, Honma T, Yamada M (1999) Effect of chelating agents on HDS and aromatic hydrogenation over CoMo-and NiW/Al2O3. Stud Surf Sci Catal 127:161–168
36. Okamoto Y (2014) Novel molecular approaches to the structure-activity relationships and unique characterizations of Co-Mo sulfide hydrodesulfurization catalysts for the production of ultra-clean fuels. Bull Chem Soc Jpn 87:20–58
37. Pashigreva A, Bukhtiyarova GA, Klimov OV, Chesalov YA, Litvak GS, Noskov AS (2010) Activity and sulfidation behavior of the CoMo/Al2O3 hydrotreating catalyst: the effect of drying conditions. Catal Today 149:19–27
38. Peña L, Valencia D, Klimova T (2014) CoMo/SBA-15 catalysts prepared with EDTA and citric acid and their performance in hydrodesulfurization of dibenzothiophene. Appl Catal B Environ 147:879–887
39. Peri J (1965) Infrared and gravimetric study of the surface hydration of γ-Alumina. J Phys Chem 69:211–219
40. Smegal J, Gabrielov AG, Wolohan P, Gillespie WD (2013) Composition and a method of making and use of such composition. US Patent 2013, 0199969 A1, 1–8. US20130199969 A1
41. Srivastava A, Gunjikar VG, Sinha APB (1987) Thermoanlytical studies of zinc citrate, bismuth citrate and calcium citrate. Thermochim Acta 117:201–217
42. Stanislaus A, Marafi A, Rana MS (2010) Recent advances in the science and technology of ultra-low sulfur diesel (ULSD) production. Catal Today 153:1–68
43. Topsøe H, Clausen BS, Massoth FE (1996) Hydrotreating Catalysis, Science and Technology. In: Boudart M (ed) Anderson J. Springer, Berlin
44. Valencia D, Klimova T (2013) Citric acid loading for MoS2-based catalysts supported on SBA-15. New catalytic material with high hydrogenolysis ability in the hydrodesulfurization. Appl Catal B Environ 129:137–145
45. van Dillen A, Terörde RJAM, Lensveld DJ, Geus JW, de Jong KP (2003) Synthesis of supported catalysts by impregnation and drying using aqueous chelated metal complexes. J Catal 216:257–264

46. Webb P, Orr C (1997) Analytical methods on fine particle technology. Micromeritics Instrument Corp, Norcross
47. Wyrzykowski D, Hebanowska E, Nowak-Wiczk G, Makowski M, Chmurzynski L (2011) Thermal behaviour of citric acid and isomeric aconitic acids. J Therm Anal Calorim 104:731–735
48. Zavyalova U, Scholz P, Ondruschka B (2007) Influence of cobalt precursor and fuels on the performance of combustion synthesized Co3O4/γ-Al2O3 catalysts for total oxidation of methane. Appl Catal A Gen 323:226–233
49. Zhang L, Tian C, Waychunas GA, Shen YR (2008) Structures and charging of α-Alumina (0001)/water interfaces studied by sum-frequency vibrational spectroscopy. J Am Chem Soc 130:7686–7694